Journal of Computational Physics 228 (2009) 7375–7387

Contents lists available at ScienceDirect

Journal of Computational Physics

journal homepage: www.elsevier.com/locate/jcp

An analytical derivation of the optimum source patterns for the pseudospectral time-domain method

Zhili Lin [a,b,*], Lars Thylén [b,c,d]

[a] School of Instrumentation Science and Optoelectronics Engineering, Beihang University, Beijing 100191, China
[b] Department of Microelectronics and Applied Physics, Royal Institute of Technology, SE-164 40 Kista, Sweden
[c] Joint Research Center of Photonics of the Royal Institute of Technology, Sweden
[d] Zhejiang University, China

ARTICLE INFO

Article history:
Received 28 April 2008
Received in revised form 22 March 2009
Accepted 29 June 2009
Available online 1 July 2009

Keywords:
Pseudospectral time-domain method
Discrete Fourier transform
Circular discrete convolution
Tailor series expansion

ABSTRACT

In the computational electromagnetics and acoustics, spatially smoothed sources are often utilized to alleviate the aliasing errors in the pseudospectral time-domain (PSTD) algorithms. In our work, an analytical derivation of the optimum source patterns is presented according to the accurately derived expressions of the dominant source-introduced aliasing errors according to the circular discrete convolution and Tailor series expansion method. We quantitatively demonstrate, for the first time in literature, that the aliasing errors can be optimally suppressed and rapidly reduced to the negligible levels by these optimum patterns and with the increment of source cells. We also provide the different implementation schemes of the optimal patterns both for the soft and hard source cases. The numerical calculation and 1D PSTD transient simulations are conducted to verify the excellent performance of these optimum sources.

1. Introduction

In recent years, the pseudospectral time-domain (PSTD) method has been widely used for solving Maxwell's equations in many electromagnetic and acoustic problems [1–4]. Unlike the traditional finite-difference time-domain (FDTD) method, PSTD uses the discrete Fourier transform (DFT), implemented by the fast Fourier transform (FFT) algorithm, to calculate the spatial derivatives of the field components with infinite order accuracy and a low sampling density of two points per wavelength at the highest frequency being simulated [1]. Therefore, it causes smaller numerical phase velocity errors as compared to the FDTD method and therefore allows problems of much greater electrical size to be modeled. Moreover, because the electric and magnetic field components are sampled at the same location, the PSTD is especially useful for simulating the wave propagation through novel metamaterials whose permittivity and permeability are both sharply changed [5]. With these and other unmentioned advantages, the march-in-time PSTD method becomes an outstanding modeling technique in the computational electromagnetics.

However, the DFT has difficulty in correctly representing a Kronecker delta function in a global basis. When we specify the source-driving values to a single source cell, the zigzag wiggles would become great apparent on the excited waves, usually referred to as the Gibbs phenomenon in the study of Fourier series [6], especially in the simulation domain near the source. These artifacts will pose a grave threat to obtaining correct simulation results and should be eliminated or reduced to negligible levels. To alleviate these aliasing errors, a spatially smoothed source occupying a volume of a few (4–6) cells in each

* Corresponding author. Address: School of Instrumentation Science and Optoelectronics Engineering, Beihang University, XueYuan Road No. 37, HaiDian District, Beijing 100191, China. Tel: +46 8 790 4266; fax: +46 8 752 7850.
E-mail addresses: zllin2008@gmail.com (Z. Lin), lthylen@kth.se (L. Thylén).

0021-9991/$ - see front matter © 2009 Elsevier Inc. All rights reserved.
doi:10.1016/j.jcp.2009.06.033

coordinate direction has been proposed by Liu [3], but without details on the source patterns. A spatially compact source spanning two cells with identical source-driving value was also investigated by Lee and Hagness [7] with many practical simulation examples. However, their study is just based on the method of comparison between single-cell and two-cell sources. The detailed guidelines for the optimum source patterns and their corresponding performances are still remaining unreported although this is a quite important issue for the PSTD method.

In this paper, the analytical expressions of the dominant aliasing errors introduced by the localized sources are first deduced based on the circular discrete convolution and the Tailor series expansion method. Then the optimum patterns of the sources with minimum levels of introduced aliasing errors can be subsequently derived and their performances can be quantitatively compared among them with the increment of source cells. Based on these optimum source patterns, the practical implementation of them for both the soft and hard source cases is further provided. For a source containing more than six cells would be much loss of compactness, only sources composed of 2–6 cells are investigated in this work.

2. Formulation for aliasing errors

Consider a 1D problem that a TEM wave propagates along the x-axis with the electric field vector oriented in the z-direction in vacuum. The 1D grid space contains N cells with referred indices starting from zero in the sequence $i = 0, 1, 2, \ldots, N-1$. Suppose the spanning source is composed of m current sheets with relative amplitudes $a_0, a_1, \ldots, a_{m-1}$ and locating on the $i_0, i_1, \ldots, i_{m-1}$th cells, respectively. According to the PSTD algorithm, the iteratively updated equations for the *normalized* electric and magnetic fields (the electric field was divided by the impedance of vacuum) is given by

$$E_z^{n+1/2} = E_z^n + c_x \boldsymbol{F}^{-1}\left\{K_x \boldsymbol{F}\left[H_y^{n+1/2}\right]\right\}, \tag{1}$$

$$E_z^{n+1} = E_z^{n+1/2} + s^{n+1/2}, \tag{2}$$

$$H_y^{n+3/2} = H_y^{n+1/2} + c_x \boldsymbol{F}^{-1}\left\{K_x \boldsymbol{F}\left[E_z^{n+1}\right]\right\}. \tag{3}$$

In the above equations, $c_x = c\Delta t/\Delta x$ is a constant of a specific problem with $c, \Delta t$ and Δx standing for the speed of light in vacuum, step time and cell size used in the PSTD simulation, respectively;

$$s^{n+1/2} = [0, \ldots, 0, a_0, a_1, \ldots, a_{m-1}, 0, \ldots, 0] f^{n+1/2}, \tag{4}$$

being the scalar source-driving matrix of size $1 \times N$ and $f^{n+1/2}$ denotes the to-be-superimposed temporal driving function on the source cells at time step $n + 1/2$; $\boldsymbol{F}$ and $\boldsymbol{F}^{-1}$ are the forward and inverse DFT defined by

$$X(k) = \sum_{i=0}^{N-1} x(i) e^{-j\frac{2\pi}{N}ik}, \quad k = 0, \ldots, N-1, \tag{5}$$

$$x(i) = \frac{1}{N}\sum_{k=0}^{N-1} X(k) e^{j\frac{2\pi}{N}ki}, \quad i = 0, \ldots, N-1, \tag{6}$$

and the differencing factor K_x is given by

$$K_x(k) = \begin{cases} j2\pi k/N, & k = 0, \ldots, N/2-1; \\ 0, & k = N/2; \\ j2\pi(k-N)/N, & k = N/2+1, \ldots, N-1. \end{cases} \tag{7}$$

One may note that (1) and (2) actually can merge together. The reason we split into two updating steps is just for the convenience of discussions and the emphasis of the impact of the superimposed item $s^{n+1/2}$ on the aliasing errors.

To the problem we concerned, it is proper to start with the assumption that before the introduction of the source item $s^{n+1/2}$ at time step $n + 1/2$, the waveform of the magnetic field $H_y^{n+1/2}$ is sufficiently smooth in space so that its spatial differencing process via (1) can be implemented without causing any perceptible aliasing errors on the whole domain. In another words, the waveform of $E_z^{n+1/2}$ in the right side of (2) is considered be to fairly smooth, so the potential abruption of E_z^{n+1} in the left side of (2) would be only coming from the introduced source item $s^{n+1/2}$. Thus the following two items

$$\sigma_H^{n+3/2} = c_x \boldsymbol{F}^{-1}\left\{K_x \boldsymbol{F}\left[s^{n+1/2}\right]\right\}, \tag{8}$$

$$\sigma_E^{n+2} = c_x \boldsymbol{F}^{-1}\left\{K_x \boldsymbol{F}\left[\sigma_H^{n+3/2}\right]\right\}, \tag{9}$$

become the dominant aliasing errors of the magnetic field and electric field introduced by $s^{n+1/2}$ on the cells away from the spanning source. We move to derive the analytical expression for $\sigma_H^{n+3/2}$ and σ_E^{n+2}. One notes that in (8) and (9), K_x only depends on N, while c_x is only determined by the stability criterion of the PSTD algorithm [1], that is $c_x = c\Delta t/\Delta x \leqslant 2/(\pi\sqrt{D})$ which D is the dimensionality of the simulation problem under study. Thus the only controllable factor to alleviate the

aliasing errors is the pattern of the source. Nevertheless, how will the different source patterns affect the aliasing errors is greatly blurred by directly applying pair of forward and inverse DFT on the source items as (8) does. Therefore, alternatively, we would utilize the discrete series convolution to do the calculation. According to the convolution theorem,

$$\boldsymbol{F}^{-1}\{K_x \cdot \boldsymbol{F}[s^{n+1/2}]\} = s^{n+1/2} * \boldsymbol{F}^{-1}[K_x] = s^{n+1/2} * k_x, \tag{10}$$

where the asterisk '$*$' denotes a circular discrete convolution operator. The exact expression of $k_x = \boldsymbol{F}^{-1}[K_x]$ can be obtained by doing the inverse DFT on (7) and its explicit analytical form [8] is

$$k_x(i) = \begin{cases} 0, & i = 0 \\ (-1)^i \alpha / \tan[\alpha \cdot i], & i = 1, \ldots, N-1, \end{cases} \tag{11}$$

with $\alpha = \pi/N$. From (11), we notice the intrinsic properties of k_x that the absolute values of all the elements of k_x are less than one,$0 \leqslant |k_x| < 1$, while the values of two adjacent elements are always opposite in sign except for those at $i = 0, \pm N/2$ where the values are zero. Based on (4) and (10), the Eq. (8) can be expanded as

$$\sigma_H^{n+3/2}(i) = c_x \sum_{p=0}^{N-1} s^{n+1/2}(p) * k_x(i-p) = c_x f^{n+1/2} \sum_{l=0}^{m-1} a_l \cdot k_x(i - i_l). \tag{12}$$

Incidentally, to implement (12), k_x can be extended to the negative cell-index range,$-N+1 \leqslant i \leqslant 0$, as follows

$$k_x(i) = k_x(N+i), \quad i = -1, -2, \ldots, -N+1,$$

due to the periodic property of circular discrete convolution.

However, for (12) is still not very straightforward, we introduce a new quantity,h_x, which is a shifting of k_x rightward by i_{m-1} elements; that is

$$h_x(i) = k_x(i - i_{m-1}), \tag{13}$$

where i_{m-1} is the cell-index of the last source cell. Then (12) can be simplified as

$$\sigma_H^{n+3/2}(i) = c_x f^{n+1/2} \sum_{l=0}^{m-1} a_l \cdot h_x(i+l) = c_x f^{n+1/2}[a_0 h_x(i) + a_1 h_x(i+1) + \cdots + a_{m-1} h_x(i+m-1)]. \tag{14}$$

In (14), the distribution of the aliasing errors of magnetic field introduced by the source item, $s^{n+1/2}$, is fairly straightforward. By doing the entry-wise product on the source pattern matrix $[a_0, a_1, \ldots, a_{m-1}]$ and the corresponding matrix $[h_x(i), h_x(i+1), \ldots, h_x(i+m-1)]$, and further multiplying the product with the constant $c_x f^{n+1/2}$, we obtain $\sigma_H^{n+3/2}(i)$. After that with (9), we can further calculate the aliasing errors of electric field by

$$\sigma_E^{n+2} = c_x\{k_x * \sigma_H^{n+3/2}\}. \tag{15}$$

Eqs. (14) and (15) are the analytical expressions of the dominant aliasing errors of the magnetic and electric field introduced by the superimposed source item, $s^{n+1/2}$.

For the sake of illustration but without loss of generality, due to the periodicity of DFT, $i_{m-1} = N/2$ is assumed, which means the last source cell locates at the center of the computational region and other source cells are on the left side of it. As an example, the location of a spatially smoothed source with $m = 5$ is shown in Fig. 1(a). Further, $f^{n+1/2} = 2$ and $c_x = 0.5$ are assumed to shorten the lengthy expressions. According to (11) and (13), the expression for h_x is given by

$$h_x(i) = \begin{cases} 0, & i = N/2, \\ (-1)^{i+1} \alpha \tan(\alpha \cdot i), & i = 0, 1, \ldots, N/2-1, N/2+1, \ldots N-1, \end{cases} \tag{16}$$

Similar to k_x, h_x can be extended to other periodic sections by

$$h_x(i) = h_x(Nl + i),$$

where l is an integer. One period of $h_x$is plotted in Fig. 1(b) for $N = 64$. For the sake of comparison, we define a new auxiliary function

$$g_x(i) = \begin{cases} 0, & i = N/2; \\ \alpha \tan(\alpha \cdot i), & i = \textit{others}. \end{cases} \tag{17}$$

The shape of g_x is also shown in Fig. 1(b) and from where we can see that its elements' absolute values are always less than 1 like those of k_x. According to (14) and the assumed parameters, the aliasing errors of magnetic field are

$$\sigma_H^{n+3/2}(i) = a_0 h_x(i) + a_1 h_x(i+1) + \cdots + a_{m-1} h_x(i+m-1), \tag{18}$$

with $i = 0, 1, \ldots, N-1$. Due to the symmetry of h_x, we note from (18) that the optimum pattern of the spatially smoothed source should be symmetric; otherwise, the aliasing errors may be alleviated to negligible levels for the cells on one side of source, but definitely will remain large for the cells on the other side of the source. This is because the absolute values

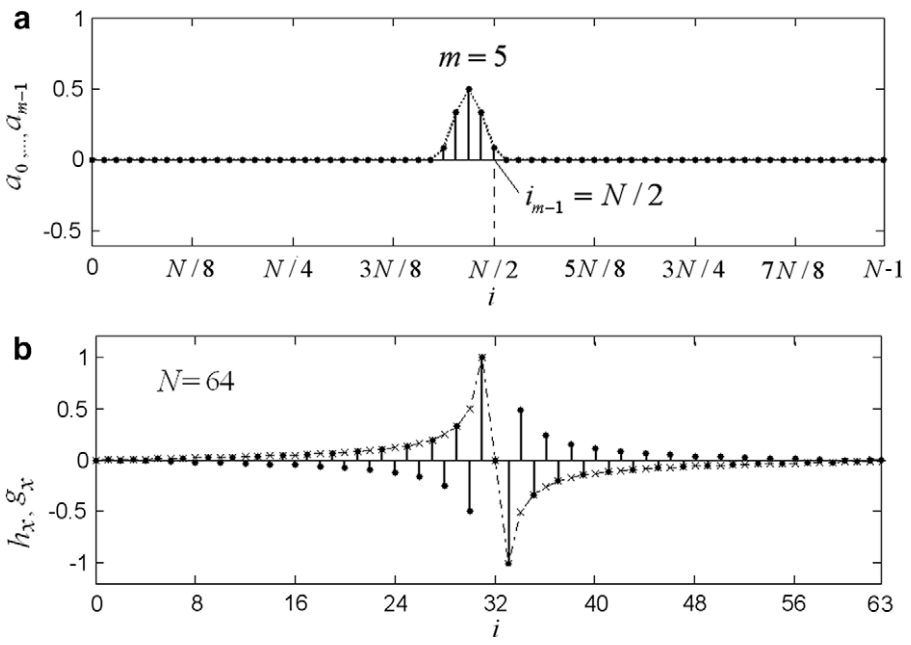

Fig. 1. (a) The exemplified location of the spatially smoothed source with $m = 5$; and (b) the stem graph of h_x for $N = 64$. The dashed line with '×' signs stands for the shape of the auxiliary function g_x.

of h_x is an increasing function in the computational domain left to source but a decreasing function in the right one. So the first principle of the optimum source pattern is the symmetry; that is

$$a_0 = a_{m-1}, \quad a_1 = a_{m-2}, \ldots, a_{m/2-1} = a_{m/2}, \quad \text{if } m \text{ is even;} \tag{19-1}$$

$$a_0 = a_{m-1}, \quad a_1 = a_{m-2}, \ldots, a_{(m+1)/2-2} = a_{(m+1)/2}, \quad \text{if } m \text{ is odd.} \tag{19-2}$$

Only when (19-1 and -2) are satisfied, the aliasing errors on the both sides of domain, right and left to the source, would be symmetric and possibly reduced to negligible levels simultaneously. To increase the comparability among the performances of different source patterns, the sum of $a_0, \ldots, a_{m-1}$ also should be normalized here that

$$a_0 + a_1 + \cdots + a_{m-2} + a_{m-1} = 1. \tag{20}$$

Since any spatially smoothed source is the result of the superposition of several single-cell sources, it is important to first investigate the property of aliasing errors introduced by a single-cell source. From (18) and (20), we have $a_0 = 1$ and

$$\sigma_H^{n+3/2}(i) = a_0 h_x(i) = (-1)^{i+1} g_x(i). \tag{21}$$

We can see that the absolute values of the aliasing errors of magnetic field on the cells away from the source are as large as those of g_x! Such as for $N = 64$, the aliasing error on cell $i = 48$ is $\sigma_E^{n+2}(48) = \alpha = 0.049$. This is the original reason why a single-cell source is problematic for a PSTD algorithm. Further from (15), we obtain [8]

$$\sigma_E^{n+2}(i) = (-1)^i \left[\frac{1}{2}(N-2)\alpha^2 - g_x^2(i)\right], \tag{22}$$

for the cells $i \neq N/2$ and $\sigma_E^{n+2}(N/2) = -\alpha^2(N-2)(N-1)/6$. That is, the aliasing errors of electric field on the cells away from the source are approximately

$$\sigma_E^{n+2}(i) \approx (-1)^i \left[\frac{1}{2}(N-2)\right]\alpha^2 \approx (-1)^i \frac{\pi}{2}\alpha.$$

These errors are unbearably large, such as for $N = 64, \sigma_E^{n+2}(48) = 30\alpha^2 = 0.072$. Based on (18), (21) and (22), we can move on to derive the aliasing errors introduced by a spanned source composed of m cells that

$$\sigma_H^{n+3/2}(i) = (-1)^{i+1} \sum_{l=0}^{m-1} (-1)^l a_l g_x(i+l), \tag{23}$$

$$\sigma_E^{n+2}(i) = (-1)^i \sum_{l=0}^{m-1} (-1)^l a_l \left\{\frac{1}{2}(N-2)\alpha^2 - g_x^2(i+l)\right\}, \tag{24}$$

According to (19-1 and -2), (23) and (24), we find that the analytical expressions for the aliasing errors introduced by a source composed of even cells are a bit different from those by an odd-cell source. Therefore, we deduce them separately according to m is even or odd. The results are a little longsome and therefore given in the Appendix A.

3. Optimum source patterns

As we can see from (2), the source item $s^{n+1/2}$ is superimposed on the previous electric field. So the performance of source patterns can be evaluated according to the aliasing errors, $\sigma_H^{n+3/2}$ and σ_E^{n+2} on the cells away from the source, whose pattern is determined by $s^{n+1/2}$. With the results obtained in Section 2 and Appendix A, we can deduce the optimum patterns of the spanning sources composed of a specific number of cells with minimum $\sigma_H^{n+3/2}$ and σ_E^{n+2} introduced.

3.1. Two-cell source ($m = 2$)

According to (19-1) and (20), we have $a_0 = a_1 = 0.5$. Further from (A.1), (A.2) and (A.3) with $t(0) = 1$, the expressions for aliasing errors by a two-identical-cell source are

$$\begin{aligned}\sigma_H^{n+3/2}(i)|_{m=2} &= (-1)^i 2\alpha\left\{a_0\left[\left(\frac{\alpha}{2}+\frac{\alpha^3}{24}\right)+\left(\frac{\alpha}{2}+\frac{\alpha^3}{6}\right)\beta^2+\frac{\alpha^3}{8}\beta^4+O(\alpha^5)\right]\right\} = (-1)^i\frac{1}{2}\left[\alpha^2+\alpha^2\beta^2+O(\alpha^4)\right]\\ &\approx (-1)^i\frac{1}{2}\left[\alpha^2+g_x^2(i+0.5)\right],\end{aligned} \tag{25}$$

$$\begin{aligned}\sigma_E^{n+2}(i)|_{m=2} &= (-1)^i 4\alpha^2\left\{a_0\left[\left(\frac{\alpha}{2}+\frac{\alpha^3}{6}\right)\beta+\left(\frac{\alpha}{2}+\frac{5\alpha^3}{12}\right)\beta^3+\frac{\alpha^3}{4}\beta^5+O(\alpha^5)\right]\right\} = (-1)^i[\alpha^3\beta+\alpha^3\beta^3+O(\alpha^5)]\\ &\approx (-1)^i\left[\alpha^2 g_x(i+0.5)+g_x^3(i+0.5)\right],\end{aligned} \tag{26}$$

where $\beta(i) = \tan(\alpha i + \alpha/2)$ and $g_x(i+0.5) = \alpha\tan(\alpha i + \alpha/2)$ in this case. Comparing (25) and (26) with (21) and (22), we can find that the magnitudes of aliasing errors of magnetic and electric fields from the two-identical-cell source are much smaller than those from the single-cell source. This is inconsistent with the results given in [7]. For example, for $N = 64$ with $\alpha = 0.049$ and $g_x(48+0.5) = -0.046$, the residual aliasing errors on the cell $i = 48$ are $\sigma_H^{n+3/2}(48) = 2.3\times10^{-3}$ and $\sigma_E^{n+2}(48) = -2.1\times10^{-4}$.

3.2. Three-cell soft source ($m = 3$)

According to (19-2) and (20), the optimum pattern for a tree-cell source would be like $[a_0, a_1, a_0]$ where $2a_0 + a_1 = 1$. From (A.4), (A.5) and (A.6) with $t(0) = 2$, the aliasing errors are

$$\begin{aligned}\sigma_H^{n+3/2}(i)|_{m=3} &= (-1)^{i+1}\alpha\left\{(2a_0-a_1)\beta+2a_0\left[\left(\alpha^2+\frac{2\alpha^4}{3}\right)\beta+\left(\alpha^2+\frac{5\alpha^4}{3}\right)\beta^3+\alpha^4\beta^5+O(\alpha^6)\right]\right\}\\ &= (-1)^{i+1}\alpha\left[(2a_0-a_1)\beta+2a_0\alpha^2(\beta+\beta^3)+O(\alpha^4)\right],\end{aligned} \tag{27}$$

$$\begin{aligned}\sigma_E^{n+2}(i)|_{m=3} &= (-1)^i\left(\frac{N-2}{2}\right)\alpha^2(2a_0-a_1)\\ &\quad+(-1)^{i+1}\alpha^2\left\{(2a_0-a_1)\beta^2+2a_0\left[\left(\alpha^2+\frac{2}{3}\alpha^4\right)+\left(4\alpha^2+\frac{17\alpha^4}{3}\right)\beta^2+(3\alpha^2+10\alpha^4)\beta^4+5\alpha^4\beta^6+O(\alpha^6)\right]\right\}\\ &= (-1)^{i+1}\alpha^2\left[(2a_0-a_1)\left(\beta^2-\frac{N-2}{2}\right)+2a_0\alpha^2(1+4\beta^2+3\beta^4)+O(\alpha^4)\right],\end{aligned} \tag{28}$$

where $\beta(i) = \tan(\alpha i + \alpha)$ for this case. From (27) and (28), to reduce the aliasing errors to minimum levels, it is optimum to set $a_1 = 2a_0$. Considering $2a_0 + a_1 = 1$, we obtain that $a_1 = 1/2, a_0 = 1/4$. Therefore, the optimum source pattern in a normalized form for a three-cell source is $[1/4, 1/2, 1/4]$, with the minimum aliasing errors approximately given by

$$\sigma_H^{n+3/2}(i)|_{m=3} \approx (-1)^{i+1}\frac{1}{2}\alpha^3[\beta+\beta^3] = (-1)^{i+1}\frac{1}{2}\left[\alpha^2 g_x(i+1)+g_x^3(i+1)\right], \tag{29}$$

$$\sigma_E^{n+2}(i)|_{m=3} \approx (-1)^{i+1}\frac{1}{2}\alpha^4[1+4\beta^2+3\beta^4] = (-1)^{i+1}\frac{1}{2}\left[\alpha^4+4\alpha^2 g_x^2(i+1)+3g_x^4(i+1)\right], \tag{30}$$

where $g_x(i+1) = \alpha\tan(\alpha i + \alpha)$. Comparing (29) and (30) with (25) and (26), we can find that the aliasing errors by a three-cell source are further suppressed because they are multiplied by the factor g_x. Such as for $N = 64$ with $\alpha = 0.049$ and $g_x(48+1) = -0.044$, the aliasing errors on the cell $i = 48$ are $\sigma_H^{n+3/2}(48) = 9.8\times10^{-5}$ and $\sigma_E^{n+2}(48) = -1.8\times10^{-5}$, about one order of magnitude smaller than those introduced by a two-identical-cell source.

3.3. Four-cell soft source (m = 4)

Likewise, the optimum pattern for a four-cell source would be something as $[a_0, a_1, a_1, a_0]$ where $2a_0 + 2a_1 = 1$. From (A.1), (A.2) and (A.3) with $t(0) = 3$ and $t(1) = 1$, the aliasing errors can be given as

$$\sigma_H^{n+3/2}(i)|_{m=4} = (-1)^i 2\alpha\left\{\left[\frac{\alpha}{2}(3a_0 - a_1) + \frac{\alpha^3}{24}\left(3^3a_0 - a_1\right)\right] + \left[\frac{\alpha}{2}(3a_0 - a_1) + \frac{\alpha^3}{6}\left(3^3a_0 - a_1\right)\right]\beta^2 + \frac{\alpha^3}{8}\left(3^3a_0 - a_1\right)\beta^4 + O(\alpha^5)]\right\}, \tag{31}$$

$$\sigma_E^{n+2}(i)|_{m=4} = (-1)^i 4\alpha^2\left\{\left[\frac{\alpha}{2}(3a_0 - a_1) + \frac{\alpha^3}{6}\left(3^3a_0 - a_1\right)\right]\beta + \left[\frac{\alpha}{2}(3a_0 - a_1) + \frac{5\alpha^3}{12}\left(3^3a_0 - a_1\right)\right]\beta^3 + \frac{\alpha^3}{4}\left(3^3a_0 - a_1\right)\beta^5 + O(\alpha^5)]\right\}, \tag{32}$$

where $\beta(i) = \tan(\alpha i + 1.5\alpha)$ in this case. From (31) and (32), we can see that when $3a_0 - a_1 = 0$ is fulfilled the aliasing errors can be reduced to minimum levels for a four-cell source. Also considering $2a_0 + 2a_1 = 1$, we have $a_0 = 1/8$ and $a_1 = 3/8$. Thus the optimum normalized profile for a four-cell source is [1/8,3/8,3/8,1/8] with the aliasing errors approximately

$$\sigma_H^{n+3/2}(i)|_{m=4} \approx (-1)^i \frac{1}{4}\alpha^4(1 + 4\beta^2 + 3\beta^4) = (-1)^i \frac{1}{4}\left[\alpha^4 + 4\alpha^2 g_x^2(i + 1.5) + 3g_x^4(i + 1.5)\right], \tag{33}$$

$$\sigma_E^{n+2}(i)|_{m=4} \approx (-1)^i \alpha^5(2\beta + 5\beta^3 + 3\beta^5) = (-1)^i\left[2\alpha^4 g_x(i + 1.5) + 5\alpha^2 g_x^3(i + 1.5) + 3g_x^5(i + 1.5)\right], \tag{34}$$

where $g_x(i + 1.5) = \alpha\tan(\alpha i + 1.5\alpha)$. Such as for $N = 64$ with $g_x(48 + 1.5) = -0.042$ and $\alpha = 0.049$, the remaining aliasing errors on the cell $i = 48$ are $\sigma_H^{n+3/2}(48) = 8.2 \times 10^{-6}$ and $\sigma_E^{n+2}(48) = -1.8 \times 10^{-6}$, much smaller than those by an optimum three-cell source.

3.4. Five-cell soft source (m = 5)

According to (19-2) and (20), the optimum pattern for a five-cell sources would have a form like $[a_0, a_1, a_2, a_1, a_0]$ with $2a_0 + 2a_1 + a_2 = 1$ being satisfied. From (A.4), (A.5) and (A.6) with $t(0) = 4$ and $t(1) = 2$, the aliasing errors for this case are

$$\sigma_H^{n+3/2}(i)|_{m=5} = (-1)^{i+1}\alpha(2a_0 - 2a_1 + a_2)\beta + (-1)^{i+1}2\alpha\left\{\left[\left(4^2a_0 - 2^2a_1\right)\frac{\alpha^2}{4} + \left(4^4a_0 - 2^4a_1\right)\frac{\alpha^4}{24}\right]\beta + \left[\left(4^2a_0 - 2^2a_1\right)\frac{\alpha^2}{4} + \left(4^4a_0 - 2^4a_1\right)\frac{5\alpha^4}{48}\right]\beta^3 + \left(4^4a_0 - 2^4a_1\right)\frac{\alpha^4}{16}\beta^5 + O(\alpha^6)\right\}, \tag{35}$$

$$\sigma_E^{n+2}(i)|_{m=5} = (-1)^{i+1}\alpha^2(2a_0 - 2a_1 + a_2)\left(\beta^2 - \frac{N-2}{2}\right) + (-1)^{i+1}2\alpha^2\left\{\left[\left(4^2a_0 - 2^2a_1\right)\frac{\alpha^2}{4} + \left(4^4a_0 - 2^4a_1\right)\frac{\alpha^4}{24}\right] + \left[\left(4^2a_0 - 2^2a_1\right)\alpha^2 + \left(4^4a_0 - 2^4a_1\right)\frac{17\alpha^4}{48})\right]\beta^2 + \left[\left(4^2a_0 - 2^2a_1\right)\frac{3\alpha^2}{4} + \left(4^4a_0 - 2^4a_1\right)\frac{5\alpha^4}{8}\right]\beta^4 + \left(4^4a_0 - 2^4a_1\right)\frac{5\alpha^4}{16}\beta^6 + O(\alpha^6)]\right\}, \tag{36}$$

where $\beta(i) = \tan(\alpha i + 2\alpha)$ in this case. From (35) and (36), to reduce the aliasing errors, it is optimum to set

$$2a_0 - 2a_1 + a_2 = 0 \quad \text{and} \quad 4^2a_0 - 2^2a_1 = 0.$$

Further considering that $2a_0 + 2a_1 + a_2 = 1$, we have $a_0 = 1/16, a_1 = 4/16, a_2 = 6/16$. Thus the optimum normalized pattern for a five-cell source is [1/16,4/16,6/16,4/16,1/16] with the residual aliasing errors approximately given by

$$\sigma_H^{n+3/2}(i)|_{m=5} \approx (-1)^{i+1}\frac{1}{2}\alpha^5\left[2\beta + 5\beta^3 + 3\beta^5\right] = (-1)^{i+1}\frac{1}{2}\left[2\alpha^4 g_x(i + 2) + 5\alpha^2 g_x^3(i + 2) + 3g_x^5(i + 2)\right], \tag{37}$$

$$\sigma_E^{n+2}(i)|_{m=5} \approx (-1)^{i+1}\frac{1}{2}\alpha^6\left[2 + 17\beta^2 + 30\beta^4 + 15\beta^6\right] = (-1)^{i+1}\frac{1}{2}\left[2\alpha^6 + 17\alpha^4 g_x^2(i + 2) + 30\alpha^2 g_x^4(i + 2) + 15g_x^6(i + 2)\right], \tag{38}$$

where $g_x(i + 2) = \alpha\tan(\alpha i + 2\alpha)$. Such as for $N = 64$ with $g_x(48 + 2) = -0.040$ and $\alpha = 0.049$, the aliasing errors on the cell $i = 48$ are $\sigma_H^{n+3/2}(48) = 7.9 \times 10^{-7}$ and $\sigma_E^{n+2}(48) = -2.2 \times 10^{-7}$, again about one order of magnitude smaller than those by a four-cell source.

3.5. Six-cell soft source (m = 6)

From (19-1) and (20), the potential optimum six-cell source pattern is $[a_0, a_1, a_2, a_2, a_1, a_0]$ and satisfies the normalized condition that $2a_0 + 2a_1 + 2a_2 = 1$. From (A.1), (A.2) and (A.3) with $t(0) = 5, t(1) = 3, t(2) = 1$, the aliasing errors are

$$\begin{aligned}\sigma_H^{n+3/2}(i)|_{m=6} = (-1)^i 2\alpha\Big\{ &\left[\frac{\alpha}{2}(5a_0 - 3a_1 + a_2) + \frac{\alpha^3}{24}\left(5^3a_0 - 3^3a_1 + a_2\right) + \frac{\alpha^5}{240}\left(5^5a_0 - 3^5a_1 + a_2\right)\right] \\ &+ \left[\frac{\alpha}{2}(5a_0 - 3a_1 + a_2) + \frac{\alpha^3}{6}\left(5^3a_0 - 3^3a_1 + a_2\right) + \frac{17\alpha^5}{480}\left(5^5a_0 - 3^5a_1 + a_2\right)\right]\beta^2 \\ &+ \left[\frac{\alpha^3}{8}\left(5^3a_0 - 3^3a_1 + a_2\right) + \frac{\alpha^5}{16}\left(5^5a_0 - 3^5a_1 + a_2\right)\right]\beta^4 + \frac{\alpha^5}{32}\left(5^5a_0 - 3^5a_1 + a_2\right)\beta^6 + O(\alpha^7)]\Big\},\end{aligned} \tag{39}$$

$$\begin{aligned}\sigma_E^{n+2}(i)|_{m=6} = (-1)^i 4\alpha^2\Big\{ &\left[\frac{\alpha}{2}(5a_0 - 3a_1 + a_2) + \frac{\alpha^3}{6}\left(5^3a_0 - 3^3a_1 + a_2\right) + \frac{17\alpha^5}{480}\left(5^5a_0 - 3^5a_1 + a_2\right)\right]\beta \\ &+ \left[\frac{\alpha}{2}(5a_0 - 3a_1 + a_2) + \frac{5\alpha^3}{12}\left(5^3a_0 - 3^3a_1 + a_2\right) + \frac{77\alpha^5}{480}\left(5^5a_0 - 3^5a_1 + a_2\right)\right]\beta^3 \\ &+ \left[\frac{\alpha^3}{4}\left(5^3a_0 - 3^3a_1 + a_2\right) + \frac{7\alpha^5}{32}\left(5^5a_0 - 3^5a_1 + a_2\right)\right]\beta^5 + \frac{3\alpha^5}{32}\left(5^5a_0 - 3^5a_1 + a_2\right)\beta^7 + O(\alpha^7)]\Big\},\end{aligned} \tag{40}$$

where $\beta(i) = \tan(\alpha i + 2.5\alpha)$ in this case. From (39) and (40), it is evident that when the following equations,

$$5a_0 - 3a_1 + a_2 = 0 \quad \text{and} \quad 5^3a_0 - 3^3a_1 + a_2 = 0,$$

are satisfied, the aliasing errors can be reduced to minimum for a six-cell source. Further with $2a_0 + 2a_1 + 2a_2 = 1$, we obtain $a_0 = 1/32, a_1 = 5/32$ and $a_2 = 10/32$. Thus the optimum normalized pattern for a six-cell source is [1/32,5/32,10/32, 10/32,5/32,1/32] with the residual aliasing errors approximately given by

$$\begin{aligned}\sigma_H^{n+3/2}(i)|_{m=6} &\approx (-1)^i \frac{1}{4}\alpha^6\left(2 + 17\beta^2 + 30\beta^4 + 15\beta^6\right) \\ &= (-1)^i \frac{1}{4}\left[2\alpha^6 + 17\alpha^4 g_x^2(i+2.5) + 30\alpha^2 g_x^4(i+2.5) + 15 g_x^6(i+2.5)\right],\end{aligned} \tag{41}$$

$$\begin{aligned}\sigma_E^{n+2}|_{m=6} &\approx (-1)^i \frac{1}{2}\alpha^7\left(17\beta + 77\beta^3 + 105\beta^5 + 45\beta^7\right) \\ &= (-1)^i \frac{1}{2}\left[17\alpha^6 g_x(i+2.5) + 77\alpha^4 g_x^3(i+2.5) + 105\alpha^2 g_x^5(i+2.5) + 45 g_x^7(i+2.5)\right],\end{aligned} \tag{42}$$

where $g_x(i+2.5) = \alpha\tan(\alpha i + 2.5\alpha)$. Such as for $N = 64$ with $g_x(48 + 2.5) = -0.038$ and $\alpha = 0.049$ the redundant aliasing errors on the cell $i = 48$ are $\sigma_H^{n+3/2}(48) = 9.4 \times 10^{-8}$and $\sigma_E^{n+2}(48) = -3.0 \times 10^{-8}$, which are the smallest for all the cases discussed up to six cells.

From the above analytical expressions and comparisons, we can induce that the optimal source pattern, $[a_0, a_1, \ldots a_{m-1}]$, is given by

$$a_l = \frac{1}{2^{m-1}}\frac{(m-1)!}{l!(m-1-l)!}, \quad l = 0, 1, \ldots, m-1, \tag{43}$$

for a m-cell soft source, at least for $2 \leqslant m \leqslant 6$. Interestingly, these optimum patterns are exactly corresponding to the normalized rows of a Pascal's triangle. With one more cell the source contains, the introduced aliasing errors decrease by a factor proportional to g_x on the cells away from the source for the optimum source patterns. So the reduction of aliasing errors on the cells far from the source is much perceptible than that on the cells near the source. In the case that the interested object is near the source, more source cells are needed to rapidly suppress the aliasing errors on the adjacent cells to the source cells. On the other hand, if the compactness of source is desired more, the source should be placed far away from the object.

4. Hard and soft source implementation

For practical applications, the optimum source patterns derived in Section 3 should be implemented to both hard and soft source cases. First, the optimum source patterns given by (43) can be immediately utilized for the soft source cases. In fact, for soft source case, (2) is given by

$$E_z^{n+1} = E_z^{n+1/2} + S_s^{n+1/2}, \tag{44}$$

where $S_s^{n+1/2}$ is the optimum soft source *to-be-superimposed* on the previous electric field $E_z^{n+1/2}$. Comparing (2) and (44), it is evident that

$$S_s^{n+1/2} = s^{n+1/2} = [0,\ldots,0,a_0,a_1,\ldots,a_{m-1},0,\ldots,0]f^{n+1/2}, \tag{45}$$

with $a_l (l = 0,\ldots,m-1)$ also determined by (43) is the solution for the soft source cases with the minimum aliasing errors. However, for the hard sources, the field values of $E_z^{n+1/2}$ on the source cells (indexed by $i_0, i_1, \ldots, i_{m-1}$) will be forcibly dragged to zeros before the hard source item $S_h^{n+1/2}$ is assigned. This destroys the smoothness of the previous electric field and subsequently different optimum source patterns are needed for each time step. Mathematically, for the hard source cases, (2) should be written as

$$E_z^{n+1} = E_z^{n+1/2} - A \circ E_z^{n+1/2} + S_h^{n+1/2}, \tag{46}$$

where

$$S_h^{n+1/2} = [0,\ldots,0,b_0^{n+1/2},b_1^{n+1/2},\ldots,b_{m-1}^{n+1/2},0,\ldots,0], \tag{47}$$

is the hard source pattern *assigned* on the source cells at each time step and

$$A = [0,0\ldots,0,1,1,\ldots 1,0,0,\ldots,0],$$

being the scalar matrix of size $1 \times N$ with the $i_0, i_1, \ldots, i_{m-1}$th entries being one and others being zeros and the hollow dot '$\circ$' between A and E_z denoting an *entry-wise* multiplication. Comparing (46) and (2), we find it is $\left(S_h^{n+1/2} - A \circ E_z^{n+1/2}\right)$, not $S_h^{n+1/2}$, that should have optimum source patterns similar to $s^{n+1/2}$ with patterns defined by (43). The field values of $E_z^{n+1/2}$ on the source cells, $A \circ E_z^{n+1/2}$, are not the same for each time step, so that the optimum patterns of $S_h^{n+1/2}$ will also change simultaneously at each time step. More specifically, based on (2), $b_0, b_1, \ldots, b_{m-1}$ should be determined by

$$b_0^{n+1/2} + b_1^{n+1/2} + \cdots + b_{m-1}^{n+1/2} = f^{n+1/2}, \tag{48}$$

and

$$\frac{b_0^{n+\frac{1}{2}} - E_z^{n+\frac{1}{2}}(i_0)}{a_0} = \frac{b_1^{n+\frac{1}{2}} - E_z^{n+\frac{1}{2}}(i_1)}{a_1} = \cdots = \frac{b_{m-1}^{n+\frac{1}{2}} - E_z^{n+\frac{1}{2}}(i_{m-1})}{a_{m-1}}. \tag{49}$$

From (48), (49) and (20), we obtain that

$$b_l^{n+1/2} = a_l\left[f^{n+1/2} - \sum_{k=0}^{m-1} E_z^{n+1/2}(i_k)\right] + E_z^{n+1/2}(l), \tag{50}$$

with $l = 0,1,\ldots,m-1$ for a m-cell hard source where a_l is defined in (43). In brief, for hard source cases, the optimum patterns of the source item $S_h^{n+1/2}$ assigned on the source cells at each time step should be calculated by (50) and implemented by (46). In fact, this is equivalent to superimpose an optimum source item

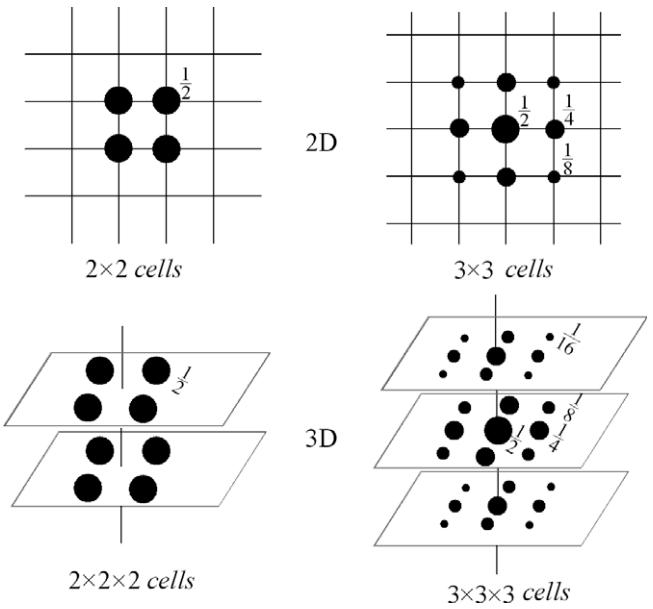

Fig. 2. The illustrations of optimum source patterns for the $2-cell$ and $3-cell$ cases in 2D and 3D problems. The sizes of the black dots imply their relative magnitudes.

$$s^{n+1/2} = \left[0,\ldots,0,d_0^{n+1/2},d_1^{n+1/2},\ldots,d_{m-1}^{n+1/2},0,\ldots,0\right], \tag{51}$$

on the previous electric field $E_z^{n+1/2}$, where $d_l^{n+1/2}$ with $l = 0,1,\ldots,m-1$ is given by

$$d_l^{n+1/2} = a_l\left[f^{n+1/2} - \sum_{k=0}^{m-1} E_z^{n+1/2}(i_k)\right]. \tag{52}$$

5. Examples and discussions

The validity of the optimum soft and hard source given in Section 4 are enough convincing as it is based on the minimum aliasing errors analytically derived in Section 3. Moreover, though being derived from 1D problem, the optimum source patterns we proposed can be easily extended to 2D and 3D cases. For example, the $2-cell$ and $3-cell$ sources in 2D and 3D problems will have the optimal patterns as illustrated in Fig. 2. We know that in the PSTD algorithm the differencing process of each field component (x, y, or z) is always actuated on only one of the three Cartesian coordinates. Therefore, as we can see from Fig. 2, if the source pattern in 1D case works optimally, its counterparts in 2D and 3D would also keep with an optimal performance. Therefore, only 1D simulation is sufficient to verify the performance of the proposed source patterns regardless the specific dimensionality, as what has partially been proved in [7] for the $2-cell$ source.

We first compare the aliasing errors introduced by the 1D sources with several optimum patterns ($m = 2,3,4,5$) under the impact of unit function $f^{n+1/2} = 1$ on the cells in the index range $40 \leqslant i \leqslant 63$ for $N = 64$. In Fig. 3, we plot the aliasing errors σ_E^{n+2} introduced by these optimum sources as functions of cell indexed in the cell range $40 \leqslant i \leqslant 63$ for $N = 64$. It is quite clear that the optimal patterns with more cells contained work better than that with fewer cells, which shows that the aliasing errors can be optimally suppressed and rapidly reduced to the negligible levels by these optimum sources and with the increment of source cells. Moreover, the PSTD calculations are also performed to evaluate the performances of the five-cell sources with the optimum pattern [1,4,6,4,1]/16 and four near-optimum patterns, say, [0.9,4,6.2,4,0.9]/16, [1.1,4,5.8,4,1.1]/16, [1,3.9995,6.001,3.9995,1]/16 and [1,4.0005,5.999,4.0005,1]/16. In Fig. 4, the aliasing errors σ_E^{n+2} introduced by these near-optimum sources are shown as functions of cell-index and all being compared with that by the optimum source. From Fig. 4, it is evident that the aliasing errors introduced by the optimum source decrease most rapidly along the cells and have the smaller values than other cases, especially on the cells far away from the source cells. We also note that the condition, $2a_0 - 2a_1 + a_2 = 0$, is very crucial for a five-cell sources with pattern $[a_0,a_1,a_2,a_1,a_0]$ and should be firstly satisfied as we can see from (A.6). This is the exact reason why a minor variation on the values of a_1 and a_2 from the

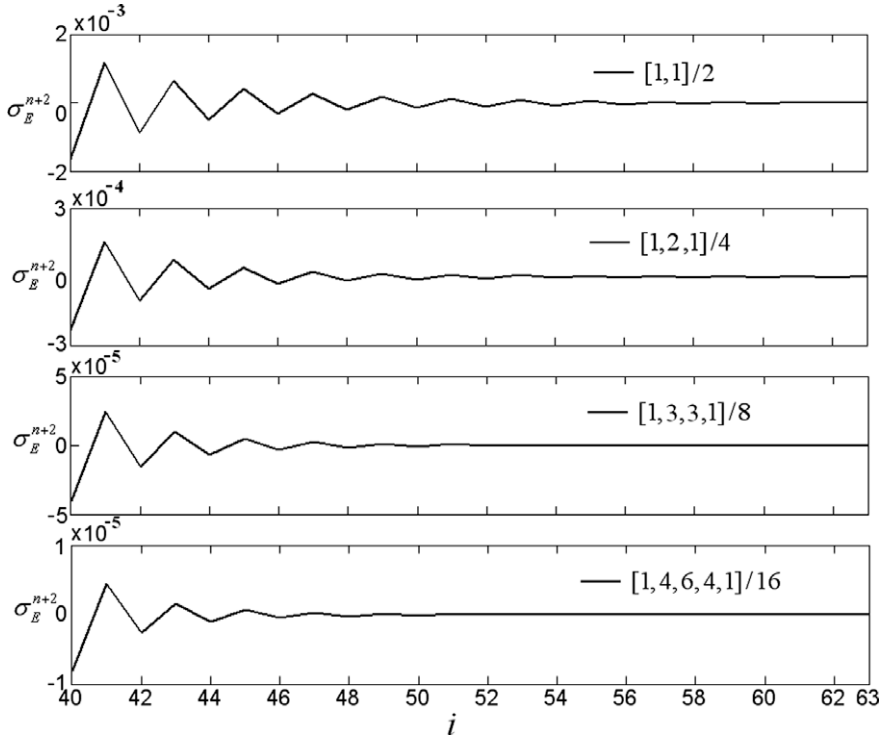

Fig. 3. The aliasing errors, σ_E^{n+2}, introduced by the 1D sources with some optimum patterns ($m = 2,3,4,5$) under the impact of unit function $f^{n+1/2} = 1$ in the cell-index range $40 \leqslant i \leqslant 63$ for $N = 64$.

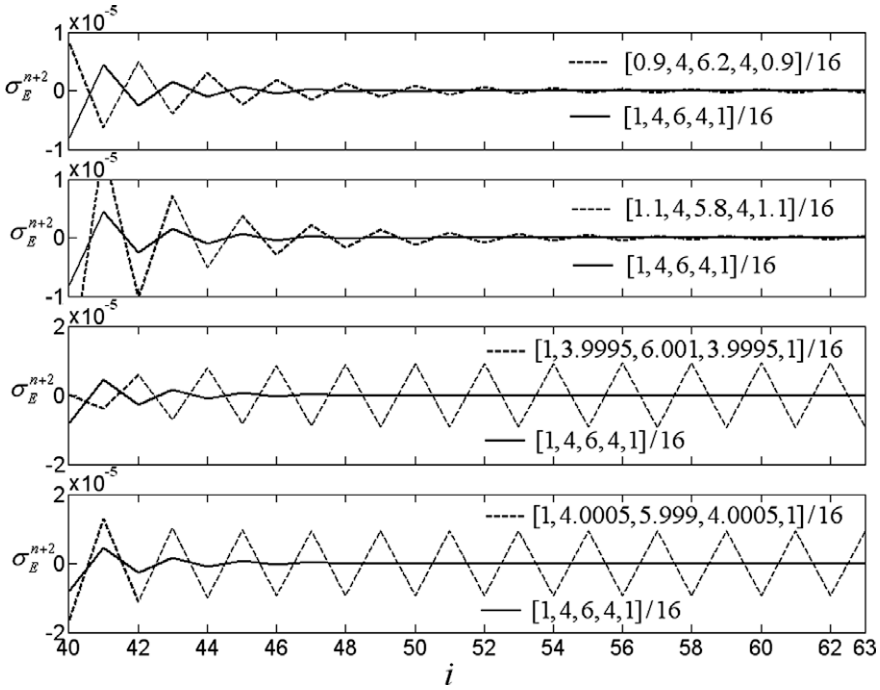

Fig. 4. The aliasing errors, σ_E^{n+2}, by the 5-cell sources with the optimum pattern and several non-optimum patterns in the cell range $40 \leqslant i \leqslant 63$ for $N = 64$.

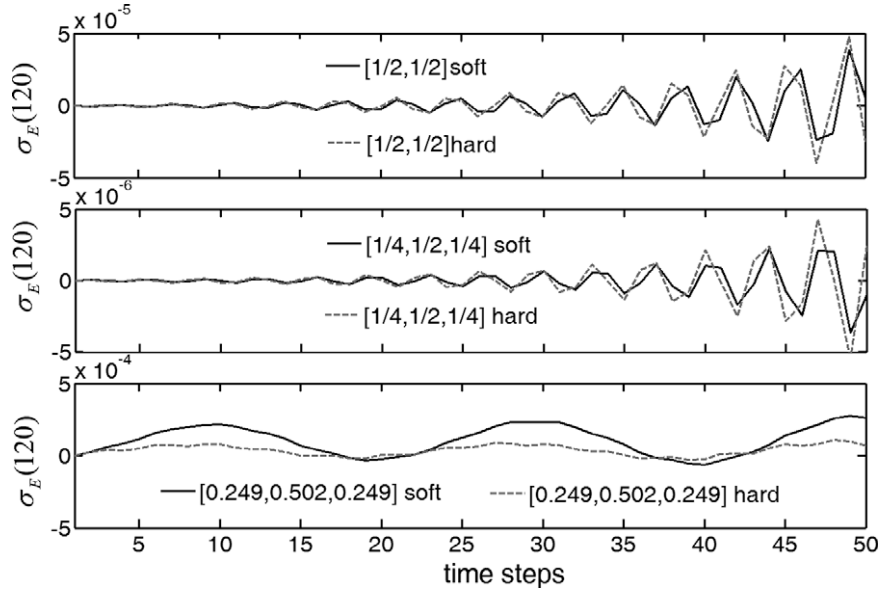

Fig. 5. The aliasing errors, σ_E, detected at the cell ($i_d = 120$), arising from the soft and hard sources with the optimum patterns [1/2, 1/2], [1/4, 1/2, 1/4] and the near-optimum pattern [0.249, 0.502, 0.249] are shown for the first 50 time steps in generating a ramped sinusoidal wave for $N = 128$.

optimum values 4/16 and 6/16, like [1, 3.9995, 6.001, 3.9995, 1]/16, will cause errors approximately as large as those with major variation on the values of a_0 and a_2, like [1.1, 4, 5.8, 4, 1.1]/16.

We further take the $2-cell$ and $3-cell$ sources as examples to evaluate and compare the performance of the proposed optimum source patterns by the 1D PSTD transient simulations. Like that in [7], a ramped sinusoidal wave, $f^{n+1/2} = \sin(0.1\pi n)\exp(0.01n)$, is used as the temporal source-driving function and the sources are placed at the center of the grid domain with $N = 128$. An artificial detector is placed on the cell ($i_d = 120$) to record the aliasing errors of electric field introduced by the to-be-tested sources in the early 50 time steps before the perceptible excited waves reach the

detector. Fig. 5 shows the simulation results of the aliasing errors from the soft and hard sources with the $2-cell$ and $3-cell$ optimum patterns[1/2, 1/2], [1/4, 1/2, 1/4] and the $3-cell$ near-optimum pattern [0.249, 0.502, 0.249] for the first 50 time steps. From Fig. 5, it is clear that the aliasing errors from the optimum hard and soft sources of the same cells are nearly equal, but the aliasing errors from the $3-cell$ optimum source is approximately one order smaller than those from the $2-cell$ optimum source and two orders smaller than those from the $3-cell$ near-optimum source [0.249, 0.502, 0.249].

Although a optimum sources composed of more cells works better, we also notice that the excited wave by a spanning source would have a temporal shape much different from the driving function not only in amplitude but also in spectrum when Δt is comparatively large. Take the soft source case as example and suppose $f_e(t)$ is the real wanted wave detected at the last source cell in the right side for a 1D problem, we have

$$f_e(t) = \sum_{l=0}^{m-1} a_l f[t - l\Delta t/c_x]. \tag{53}$$

Base on the Fourier transform, the spectrum of $f_e(t)$ is

$$F_e(\omega) = F(\omega) \sum_{l=0}^{m-1} a_l \exp[-j\omega l\Delta t/c_x], \tag{54}$$

where $F(\omega)$ is the spectrum of the driving function $f(t)$. Thus to precisely excite an expected wave $f_e(t)$ by a soft source, the driving function should be

$$f(t) = \boldsymbol{F}^{-1}[F(\omega)] = \boldsymbol{F}^{-1}\left\{ \boldsymbol{F}[f_e(t)] \Big/ \sum_{l=0}^{m-1} a_l \exp[-j\omega l\Delta t/c_x] \right\}. \tag{55}$$

In practice, $f(t)$ can be accurately calculated via (55) in advance with its discrete data $f^{n+1/2}$ stored in a matrix with a size the same as the total time steps and then conveniently utilized in the simulating iterations through the look-up-table method.

6. Conclusion

With the help of the circular discrete convolution and Tailor series expansion method, the analytical expressions for the dominant aliasing errors introduced by the spanning sources in PSTD algorithm are successfully deduced. Based on these expressions, the corresponding optimum patterns with 2–6 cells for the soft and hard sources can be easily deduced in order to alleviate the Gibbs phenomenon to levels as low as possible. We find that the spatially smoothed source with optimum patterns composed of one more cell, as a trade-off for its compactness, the aliasing errors reduced with a factor proportional to g_x on the cells away from the source. Some practical PSTD calculations and simulations are also performed to demonstrate the validity of our proposals. In practice, both accuracy and compactness need to be considered to decide how many source cells is the best for a specific problem. However, above all, the optimum patterns should always be followed regardless the number of source cells used and, as shown in Section 4, we also need to take care of the different schemes in manipulating these optimum patterns into the soft and hard working modes.

Acknowledgments

This work was partially supported by 111 Project (under Grant No. B07031) and partially supported by the program between the China Scholarship Council and the Royal Institute of Technology (KTH), Sweden. The authors also wish to thank the reviewers for their helpful comments.

Appendix A. Expressions for aliasing errors

When the source cell number m is even, according to (18) and (23) and with Taylor series expansion we have

$$\begin{aligned}
\sigma_H^{n+3/2}(i) &= (-1)^{i+1}\alpha \sum_{l=0}^{m-1} (-1)^l a_l \tan[\alpha(i+l)] = (-1)^i \alpha \sum_{l=0}^{m/2-1} (-1)^l a_l \{\tan[\alpha i + \alpha(m-l-1)] - \tan(\alpha i + \alpha l)\} \\
&= (-1)^i \alpha \sum_{l=0}^{m/2-1} (-1)^l a_l \left(\frac{\beta+\gamma}{1-\beta\gamma} - \frac{\beta-\gamma}{1+\beta\gamma} \right) \\
&= (-1)^i 2\alpha \sum_{l=0}^{m/2-1} (-1)^l a_l [\gamma + (\gamma+\gamma^3)\beta^2 + (\gamma^3+\gamma^5)\beta^4 + (\gamma^5+\gamma^7)\beta^6 + (\gamma^7+\gamma^9)\beta^8 + O(\gamma^9\beta^{10})\},
\end{aligned} \tag{A.1}$$

where

$$\beta(i) = \tan\left[\alpha i + \frac{\alpha(m-1)}{2}\right] \quad \text{and} \quad \gamma(l) = \tan\left[\frac{\alpha}{2}(m-1-2l)\right].$$

By further expanding the coefficient items to β, we also have

$$\gamma = \frac{\alpha}{2}t + \frac{\alpha^3}{24}t^3 + \frac{\alpha^5}{240}t^5 + \frac{17\alpha^7}{40320}t^7 + O(\alpha^9 t^9), \tag{A.2-1}$$

$$\gamma + \gamma^3 = \frac{\alpha}{2}t + \frac{\alpha^3}{6}t^3 + \frac{17\alpha^5}{480}t^5 + \frac{31\alpha^7}{5040}t^7 + O(\alpha^9 t^9), \tag{A.2-2}$$

$$\gamma^3 + \gamma^5 = \frac{\alpha^3}{8}t^3 + \frac{\alpha^5}{16}t^5 + \frac{3\alpha^7}{160}t^7 + O(\alpha^9 t^9), \tag{A.2-3}$$

$$\gamma^5 + \gamma^7 = \frac{a^5}{32}t^5 + \frac{\alpha^7}{48}t^7 + O(\alpha^9 t^9). \tag{A.2-4}$$

where $t(l) = (m - 1 - 2l)$ for $l = 0, 1, \ldots, m/2 - 1$. As for $\sigma_E^{n+2}(i)$, based on (18) and (24) and due to the symmetry of source pattern, it has the analytical expression

$$\begin{aligned}
\sigma_E^{n+2}(i) &= (-1)^i \left(\frac{N-2}{2}\right)\alpha^2 \sum_{l=0}^{m-1}[(-1)^l a_l] + (-1)^{i+1}\alpha^2 \sum_{l=0}^{m-1}(-1)^l a_l[\tan^2(\alpha i + l\alpha)] \\
&= (-1)^i \alpha^2 \sum_{l=0}^{m/2-1}(-1)^l a_l\{\tan^2[\alpha i + \alpha(m-l-1)] - \tan^2(\alpha i + \alpha l)\} \\
&= (-1)^i \alpha^2 \sum_{l=0}^{m/2-1}(-1)^l a_l\left[\left(\frac{\beta+\gamma}{1-\beta\gamma}\right)^2 - \left(\frac{\beta-\gamma}{1+\beta\gamma}\right)^2\right] \\
&= (-1)^i 4\alpha^2 \sum_{l=0}^{m/2-1}(-1)^l a_l[(\gamma+\gamma^3)\beta + (\gamma + 3\gamma^3 + 2\gamma^5)\beta^3 + (2\gamma^3 + 5\gamma^5 + 3\gamma^7)\beta^5 + (3\gamma^5 + 7\gamma^7 + 4\gamma^9)\beta^7 + O(\gamma^7\beta^9)].
\end{aligned} \tag{A.3}$$

Continuing with (A.2), we have

$$\gamma + 3\gamma^3 + 2\gamma^5 = \frac{\alpha}{2}t + \frac{5\alpha^3}{12}t^3 + \frac{77\alpha^5}{480}t^5 + \frac{11\alpha^7}{252}t^7 + O(\alpha^9 t^9), \tag{A.2-5}$$

$$2\gamma^3 + 5\gamma^5 + 3\gamma^7 = \frac{\alpha^3}{4}t^3 + \frac{7\alpha^5}{32}t^5 + \frac{\alpha^7}{10}t^7 + O(\alpha^9 t^9), \tag{A.2-6}$$

$$3\gamma^5(l) + 7\gamma^7(l) + 4\gamma^9(l) = \frac{3\alpha^5}{32}t^5 + \frac{3\alpha^7}{32}t^7 + O(\alpha^9 t^9). \tag{A.2-7}$$

However, when the source cell number m is odd, based on (18) and (23) and Taylor series expansion, we have

$$\begin{aligned}
\sigma_H^{n+3/2}(i) &= (-1)^{i+1}\alpha \sum_{l=0}^{m-1}(-1)^l a_l \tan[\alpha(i+l)] \\
&= (-1)^{i+1}\alpha\left\{S_1 + \sum_{l=0}^{(m-3)/2}(-1)^l a_l\{\tan[\alpha i + \alpha(m-l-1)] + \tan(\alpha i + \alpha l)\}\right\} \\
&= (-1)^{i+1}\alpha\left[S_1 + \sum_{l=0}^{(m-3)/2}(-1)^l a_l\left(\frac{\beta+\gamma}{1-\beta\gamma} + \frac{\beta-\gamma}{1+\beta\gamma}\right)\right] \\
&= (-1)^{i+1}\alpha\left\{S_1 + \sum_{l=0}^{(m-3)/2}(-1)^l 2a_l[(1+\gamma^2)\beta + (\gamma^2+\gamma^4)\beta^3 + (\gamma^4+\gamma^6)\beta^5 + (\gamma^6+\gamma^8)\beta^7 + O(\gamma^8\beta^9)]\right\},
\end{aligned} \tag{A.4}$$

where $S_1 = (-1)^{(m-1)/2}a_{(m-1)/2}\beta$ and still $\beta(i) = \tan\left[\alpha i + \frac{\alpha(m-1)}{2}\right]$ and $\gamma(l) = \tan\left[\frac{\alpha}{2}(m-1-2l)\right]$. Similarly, expanding the coefficient items gives

$$\gamma^2 = \frac{\alpha^2}{4}t^2 + \frac{\alpha^4}{24}t^4 + \frac{17\alpha^6}{2880}t^6 + \frac{31\alpha^8}{40,320}t^8 + O(\alpha^{10}t^{10}), \tag{A.5-1}$$

$$\gamma^2 + \gamma^4 = \frac{\alpha^2}{4}t^2 + \frac{5\alpha^4}{48}t^4 + \frac{77\alpha^6}{2880}t^6 + \frac{11\alpha^8}{2016}t^8 + O(\alpha^{10}t^{10}), \tag{A.5-2}$$

$$\gamma^4+\gamma^6=\frac{\alpha^4}{16}t^4+\frac{7\alpha^6}{192}t^6+\frac{\alpha^8}{80}t^8+O(\alpha^{10}t^{10}), \tag{A.5-3}$$

$$\gamma^6+\gamma^8=\frac{\alpha^6}{64}t^6+\frac{3\alpha^8}{256}t^8+O(\alpha^{10}t^{10}), \tag{A.5-4}$$

where $t(l)=(m-1-2l)$ for $l=0,1,\ldots,(m-3)/2$. As for $\sigma_E^{n+2}(i)$, based on (18) and (24), it has the following analytical expression

$$\begin{aligned}\sigma_E^{n+2}(i)&=S_2+(-1)^{i+1}\alpha^2\sum_{l=0}^{m-1}(-1)^l a_l[\tan^2(\alpha i+l\alpha)]\\&=S_2+(-1)^{i+1}\alpha^2\left\{S_3+\sum_{l=0}^{(m-3)/2}(-1)^l a_l\{\tan^2[\alpha i+\alpha(m-l-1)]+\tan^2(\alpha i+\alpha l)\}\right\}\\&=S_2+(-1)^{i+1}\alpha^2\left\{S_3+\sum_{l=0}^{(m-3)/2}(-1)^l a_l\left[\left(\frac{\beta+\gamma}{1-\beta\gamma}\right)^2+\left(\frac{\beta-\gamma}{1+\beta\gamma}\right)^2\right]\right\}\\&=S_2+(-1)^{i+1}\alpha^2\left\{S_3+\sum_{l=0}^{(m-3)/2}(-1)^l 2a_l[\gamma^2+(1+4\gamma^2+3\gamma^4)\beta^2+(3\gamma^2+8\gamma^4+5\gamma^6)\beta^4\right.\\&\quad\left.+\left(5\gamma^4+12\gamma^6+7\gamma^8)\beta^6+(7\gamma^6+16\gamma^8+9\gamma^{10})\beta^8+O(\gamma^8\beta^{10})\right\},\end{aligned} \tag{A.6}$$

where $S_2=(-1)^i\left(\frac{N-2}{2}\right)\alpha^2\left[(-1)^{(m-1)/2}a_{(m-1)/2}+2\sum_{l=0}^{(m-3)/2}(-1)^l a_l\right]$ and $S_3=(-1)^{(m-1)/2}a_{(m-1)/2}\beta^2$. Continuing with (A.5), we have

$$4\gamma^2+3\gamma^4=\alpha^2t^2+\frac{17\alpha^4}{48}t^4+\frac{31\alpha^6}{360}t^6+\frac{691\alpha^8}{40,320}t^8+O(\alpha^{10}t^{10}), \tag{A.5-5}$$

$$3\gamma^2+8\gamma^4+5\gamma^6=\frac{3\alpha^2}{4}t^2+\frac{5\alpha^4}{8}t^4+\frac{21\alpha^6}{80}t^6+\frac{53\alpha^8}{627}t^8+O(\alpha^{10}t^{10}), \tag{A.5-6}$$

$$5\gamma^4+12\gamma^6+7\gamma^8=\frac{5\alpha^4}{16}t^4+\frac{7\alpha^6}{24}t^6+\frac{37\alpha^8}{256}t^8+O(\alpha^{10}t^{10}), \tag{A.5-7}$$

$$7\gamma^6+16\gamma^8+9\gamma^{10}=\frac{7\alpha^6}{64}t^6+\frac{15\alpha^8}{128}t^8+O(\alpha^{10}t^{10}). \tag{A.5-8}$$

Because the constant α is often with a small value, the square of it become much smaller. For example, $\alpha^2=0.0024$ for $N=64$. Therefore, in fact, the items with powers of α larger than that of β can be neglected with a good approximation to the exact values in above equations.

References

[1] Q.H. Liu, The PSTD algorithm: a time-domain method requiring only two cells per wavelength, Microwave Opt. Technol. Lett. 15 (1997) 158–165.
[2] Q.H. Liu, Review of PSTD methods for transient electromagnetics, Int. J. Numer. Model. 17 (2004) 299–323.
[3] Q.H. Liu, Large-scale simulations of electromagnetic and acoustic measurements using the pseudospectral time-domain (PSTD) algorithm, IEEE Trans. Geosci. Remote Sensing 37 (1999) 917–926.
[4] G.-X. Fan, Q.H. Liu, Pseudospectral time-domain algorithm applied to electromagnetic scattering from electrically large objects, Microwave Opt. Technol. Lett. 29 (2001) 123–125.
[5] M.W. Feise, J.B. Schneider, P.J. Bevelacqua, Finite-difference and pseudospectral time-domain methods applied to backward-wave metamaterials, IEEE Trans. Antennas Propagat. 52 (2004) 2955–2962.
[6] T.W. Korner, Fourier Analysis, Cambridge University Press, Cambridge, UK, 1988.
[7] T.-W. Lee, S.C. Hagness, A compact wave source condition for the pseudospectral time-domain method, IEEE Antenna Wireless Propagat. Lett. 3 (2004) 253–256.
[8] B. Conolly, I.J. Good, A table of discrete Fourier transform pairs, SIAM J. Appl. Math. 32 (1977) 810–822.